https://doi.org/10.5194/egusphere-2026-1137
Preprint. Discussion started: 7 April 2026

From Surface processes to Marine Ice-Sheet Instability: The Collapse of the Barents–Kara Ice Sheet during the last deglaciation

Victor van Aalderen[1,2,3], Sylvie Charbit[1,2], Aurélien Quiquet[1,2] and Christophe Dumas[1,2]

[1]Laboratoire des Sciences du Climat et de l'Environnement (LSCE), CEA, CNRS, UVSQ, Université Paris-Saclay, Gif-sur-Yvette, France

[2]Institut Pierre-Simon Laplace (IPSL), Université Versailles Saint-Quentin, Guyancourt, France

[3]Institut des Géosciences de l'Environnement (IGE), Université Grenoble Alpes, CNRS, IRD, INRAE, Grenoble INP, Grenoble, France.

Corresponding author: Victor van Aalderen (victor.van-aalderen@univ-grenoble-alpes.fr)

https://doi.org/10.5194/egusphere-2026-1137
Preprint. Discussion started: 7 April 2026

Abstract

During the last deglaciation, the Barents-Kara Ice Sheet (BKIS), a marine-based sector of the Eurasian Ice Sheet, was subject to a drastic retreat over only a few centuries. While the timing of the BKIS deglaciation is well documented, the mechanisms driving the ice-sheet retreat remain debated. Using the GRISLI2.0 ice sheet model, we investigate the behavior of BKIS during this period and identify the marine ice sheet instability (MISI) as the primary driver of the BKIS collapse. Contrary to current interpretations found in the literature, which suggest that a MISI is primarily initiated by ocean-induced basal melting, our results suggest that surface processes, particularly atmospheric warming, can directly trigger such a dynamic instability. Our results highlight the combined roles of atmospheric and oceanic forcings, with atmospheric warming triggering the initial retreat at the onset of the deglaciation and oceanic processes subsequently controlling its dynamics. We therefore encourage future studies on marine ice sheets instability, to give a better consideration to variations in atmospheric conditions on their impact on ice sheet destabilization.

Plain Language Summary

The last deglaciation provides a unique opportunity to study the processes driving large-scale ice sheet collapse. However, the mechanisms behind the retreat of the Barents-Kara Ice Sheet remain debated. Here, we use an ice sheet model to show that the collapse was caused by a mechanical instability triggered by rising atmospheric temperatures.

1 Introduction

During the Last Glacial Maximum (LGM, i.e. 21 ka), the Barents-Kara Ice Sheet (BKIS), which was part of the Eurasian Ice Sheet (EIS), covered a large part of the Barents and Kara Seas (Fig. S1), with a maximum ice volume of approximatively 3×10^6 km^3 (Peltier et al., 2015, Tarasov et al., 2014, Fig. S1) and up to 7 m in SLE (sea level equivalent, Hughes et al., 2016). Between the LGM and the preindustrial period, the Arctic region experienced a significant warming of at least 12°C and more than 20°C across the BKIS (Tierney et al., 2020; Annan et al., 2022). At the same time, the North Atlantic Ocean surface temperatures also increased by 2 to 7.5°C (Tierney et al., 2020; Annan et al., 2022). The BKIS began to retreat between 26 and 19 ka and fully retreated around 10 ka (Hughes et al., 2016, Peltier et al., 2015, Tarasov et al., 2014).

The BKIS was partially lying below sea level (Amante et al., 2009), making it potentially sensitive to oceanic condition variations. As the last deglaciation is one of the best documented paleoclimatic period, it offers a solid basis for comparing simulations and observations. Studying the BKIS behavior during this period is therefore a key test for understanding ice-sheet destabilization mechanisms that could also occur in the future in the West Antarctic Ice Sheet (WAIS; Mercer, 1970; DeConto and Pollard, 2016; IPCC, 2021). In particular, the WAIS is also known to be potentially susceptible to abrupt and irreversible retreat in the coming decades (DeConto and Pollard, 2016; IPCC, 2021).

The mechanism of marine ice sheets destabilization was first identified by Mercer (1970) in the West Antarctic ice sheet (WAIS) and is known as the marine ice sheet instability (MISI). This instability is related to the fact that the ice flux at the grounding line is positively correlated with the ice thickness. When the bedrock upstream of the grounding line shows a retrograde slope, an initial grounding line retreat is further amplified due to the increased ice flux. The MISI is a self-sustained instability that can only be tempered by ice-shelf buttressing (Schoof, 2012; Goldberg et al. 2009).

Marine sediment cores provide crucial insights into the timing and mechanisms of the BKIS retreat. For example, using a revised radiocarbon chronology from a Norwegian Sea sediment core, Brendryen et al. (2020) suggested that the rapid collapse of the marine-based sectors of the BKIS contributed significantly to the abrupt sea-level rise during Meltwater Pulse 1A (~14.6 ka; Fairbanks et al., 1989; Deschamps et al., 2012). This study also suggested that the abrupt retreat of the BKIS occurred just after an increase in subsurface ocean temperatures. They consequently considered that oceanic forcing played a primary role in driving the rapid destabilization of the ice sheet. However, because climate reconstructions proposed in Brendryen et al. (2020), in particular those of subsurface temperatures, were not used to force an ice-sheet model, it is difficult to assess whether these increases in ocean temperatures could have actually triggered the retreat of the BKIS.

Recent modeling studies (Petrini et al., 2020; Alvarez-Solas et al., 2019) have investigated the respective roles of atmospheric and oceanic forcings in driving the retreat of the BKIS, highlighting a predominant role of ocean warming in triggering its collapse. Both studies, however, do not include a representation of grounding line dynamics (Tsai et al., 2015) in the ice-sheet model, which may have introduced biases in the simulated deglaciation dynamics, given the largely marine-based configuration of the BKIS. As outlined in van Aalderen et al. (2024), their experimental designs also do not allow a clear quantification of the respective contributions of atmospheric and oceanic forcing, nor of the potential role of mechanical instabilities. Moreover, the methodologies adopted in these studies likely overestimate the impact of oceanic forcing on BKIS retreat (van Aalderen et al., 2024). In addition, the reconstructed climate used to force the ice-sheet model is derived either from three sub-regions (Petrini et al., 2020) or from a single region (Alvarez-Solas et al., 2019). This results in applying the same climate variability in all the grid points of the region or sub-region.

In their previous paper, van Aalderen et al. (2024) conducted a series of idealized experiments by applying constant perturbations in basal melting and atmospheric temperatures to LGM equilibrium states of the BKIS using a state-of-the-art ice sheet model including a representation of grounding line dynamics (Tsai et al., 2015). They suggest that the retreat of the ice sheet likely began in the Bjørnøyrenna and Svyataya Anna regions (Fig. S1) in response to increasing atmospheric temperatures. However, this study did not account for the actual evolution of climate during the last deglaciation. Yet, the temporal trajectory of climate change can significantly affect the deglaciation dynamics of the BKIS and may ultimately assign a more important role to either the ocean or the atmosphere in driving ice loss.

Consequently, the different modeling studies (Petrini et al., 2020; Alvarez-Solas et al., 2019; van Aalderen et al., 2024) do not allow a clear assessment of the respective contributions of atmospheric forcing, oceanic forcing, and dynamic processes such as the MISI in driving the BKIS deglaciation. Here we propose new experiments to investigate explicitly the role of different mechanisms potentially responsible for the BKIS retreat during the last deglaciation, such as changes in surface mass balance (SMB) and basal melting, and dynamic processes. Specific protocols are designed to disentangle the respective contributions of these factors to the BKIS retreat. Our approach is based on an ice-sheet model that incorporates mechanisms capable of simulating mechanical instabilities at the grounding line. To account for local climate variability, our simulations are driven by a temporally evolving local climatology that reflects the dynamics of the last deglaciation at each grid point of the model domain

2 Methods

2.1 The GRISLI ice sheet model

In this work, we used the GRISLI2.0 (hereafter, GRISLI) ice-sheet model fully described in Quiquet et al. (2018). The model is run on a Cartesian grid (20 km × 20 km) to simulate the BKIS retreat from 21 to 10 ka. GRISLI has demonstrated its ability to reproduce the grounding line migration of the Antarctic ice sheet over several glacial-interglacial cycles (Quiquet et al., 2018; Ritz et al., 2001) and has been employed in several international intercomparison exercises for shorter time scales, including both Greenland and Antarctica (e.g., Goelzer et al., 2020; Seroussi et al., 2020). Recently, it was also used to simulate the sensitivity of the Eurasian ice sheet to variations in atmospheric and oceanic temperatures (van Aalderen et al., 2024).

Changes in ice thickness with time are given by the following mass balance equation:

$$\frac{\partial H}{\partial t} = SMBB - \boldsymbol{\nabla}(\boldsymbol{U}H) \qquad (1)$$

with H the ice thickness, U the ice velocity, SMBB the sum of SMB and the basal melting (ice grounded and ice shelves), and $\nabla(UH)$ the ice flux divergence.

Calving is based on a thickness threshold of 250 m below which ice is calved. The GRISLI model also accounts for isostatic adjustment, represented by an elastic lithosphere-relaxed asthenosphere model (Le Meur and Huybrechts, 1996).

For temperate-based grounded ice, we impose a linear basal friction law as follow (Brondex et al., 2017):

$$\tau_b = -\beta u_b \qquad (2)$$

where τ_b is the basal shear stress, u_b is the basal ice velocity and β is the basal drag coefficient. In our model, β depends on the effective pressure N and on bed conditions and is expressed as $\beta = C_f \cdot C_{sedim} \cdot N$, where C_f is an internal constant parameter. The coefficient C_{sedim} accounts for the presence of subglacial sediments and takes values of 0.1 or 1 depending on the sediment thickness (Laske, 1997). N is governed by the subglacial hydrology, which is computed according to Darcy's law (Quiquet et al., 2018). We fixed a lower bound of the basal drag coefficient, β_{min}=10 *Pa.s.m*$^{-1}$, to prevent excessively fast ice flow and ensures the preservation of grounded ice in warm-based areas. For ice shelves, basal friction is neglected.

The GRISLI model used in this study is based on the same parameter settings and parametrizations as those of van Aalderen et al., 2024 (see also Tables S1 and S2), inlcuding the prescribed ice flux at the grounding line, expressed as a function of the ice thickness to the power of five, following Tsai et al. (2015).

2.2 Climate forcing

2.2.1 Climate forcing parameterization

The climatic forcing that drives the ice sheet evolution is derived from five different PMIP3/PMIP4 LGM climates, i.e. MPI-ESM-P, MIROC-ESM, IPSL-CM5A-LR, IPSL-CM5A2 and MPI-ESM1.2 (Adloff et al., 2018; Sueyoshi et al., 2013; Dufresne et al., 2013; Sepulchre et al., 2020; Mauritsen et al., 2019; Table S3). The PMIP models were chosen for their ability to provide a forcing climate enabling GRISLI to simulate ice thickness and extent (van Aalderen et al., 2024, see Figs.S2-S3 herein) in a reasonable agreement with the geologically constrained ice thickness BKIS reconstructions at the LGM based on inverse modeling approaches constrained by GPS data or based on evidence found in the existing literature (e.g. Hughes et al., 2016; Peltier et al., 2015; Tarasov et al., 2014).

To address the resolution mismatch between the PMIP LGM climate and GRISLI, the output from the climate models are resampled onto the ice sheet model grid using a bi-linear interpolation. Additionally, to correct for differences in orography due to the interpolation, a constant vertical temperature gradient is applied on the surface air temperatures. van Aalderen et al. (2024) indicate that the lapse rate plays only a very minor role in the retreat of the BKIS. Based on this result, we decided to set the lapse rate to the fixed value of 7 °C km^{-1}.

Ablation is calculated using a positive degree day (PDD) method, as formulated by Tarasov and Peltier (2002). Snow accumulation is computed from the total precipitation, interpolated on the GRISLI grid, for months with average temperatures below the melting point.

Following the approach of Pollard and DeConto (2012), the sub-shelf melt rate (OM) is determined based on ocean temperature and salinity using the formula:

$$OM = \frac{K_t \rho_w C_w}{\rho_i L_f} \left| T_o - T_f \right| \left(T_o - T_f \right) \quad (3)$$

where K_t is the constant transfer factor, set to 7 m yr^{-1} °C^{-1} in the baseline simulations as in Pollard and DeConto (2012). In this equation, ρ_w represents the density of ocean water, ρ_i is the density of ice, L_f is the latent heat of fusion of ice, C_w is the specific heat capacity of ocean water, and T_o is the local ocean temperature coming from PMIP3/4 simulations. The freezing point temperature T_f, which depends on ocean salinity and the ocean depth, is calculated using the parameterization from Beckmann and Goosse (2003).

https://doi.org/10.5194/egusphere-2026-1137
Preprint. Discussion started: 7 April 2026

In the GRISLI model, each grid point is classified as either floating or grounded ice. To account for enhanced sub-shelf melt rates near the grounding line (Beckmann and Goosse, 2003), which arise from small-scale processes not explicitly resolved by the ice-sheet model, we apply a fraction of the melt rate from adjacent floating ice to the last grounded grid point.

As PMIP models do not provide oceanic data beneath ice shelves, we performed for each vertical layer of the oceanic models a horizontal extrapolation of temperature and salinity within ten sectors corresponding to drainage basins to estimate sub-shelf melt. Further information about this approach can be found in van Aalderen et al. (2024).

2.2.2 PMIP3/4 simulations compared to reconstructions

The fives selected PMIP3/4 models were also compared to reconstructions to see their capacity to simulate the LGM and pre-industrial conditions. To this aim, we use Tierney et al. (2020) and Annan et al. (2022) reconstructions of LGM temperatures. Both studies employ broadly similar data assimilation approaches to reconstruct Last Glacial Maximum (LGM) temperatures. However, the methodology of Annan et al. (2022) differs notably in the choice of the prior, which is based on an ensemble of 31 climate model simulations drawn from multiple phases of the PMIP archive, whereas Tierney et al. (2020) use only CESM as their baseline. This difference leads to a substantially weaker global mean LGM cooling in Annan et al. (2022) (−4.5 ± 0.9 °C) compared to Tierney et al. (2020) (−6.1 °C), and results in regional discrepancies of up to ~15 °C over the BKIS region (Fig 1a) and a ~5 °C difference in warming at the surface of the Norwegian Sea (Fig. 1b).

Furthermore, surface air temperature anomalies simulated by the five PMIP simulations selected in our study range between −14°C and −23°C (Fig. 1), spanning the range between Annan et al. (2022) and Tierney et al. (2020) estimation. Specifically, IPSL-CM5A, IPSL-CM5A2, and MPI-ESM1.2 show anomalies more consistent with Annan et al. (2022), whereas the other models align better with Tierney et al. (2020).

Regarding sea surface temperatures (SST), the SSTs simulated by the selected PMIP models are globally of the same order of magnitude as the reconstructions of Tierney et al. (2020), and consequently strongly underestimate the warming compared to Annan et al. (2022).

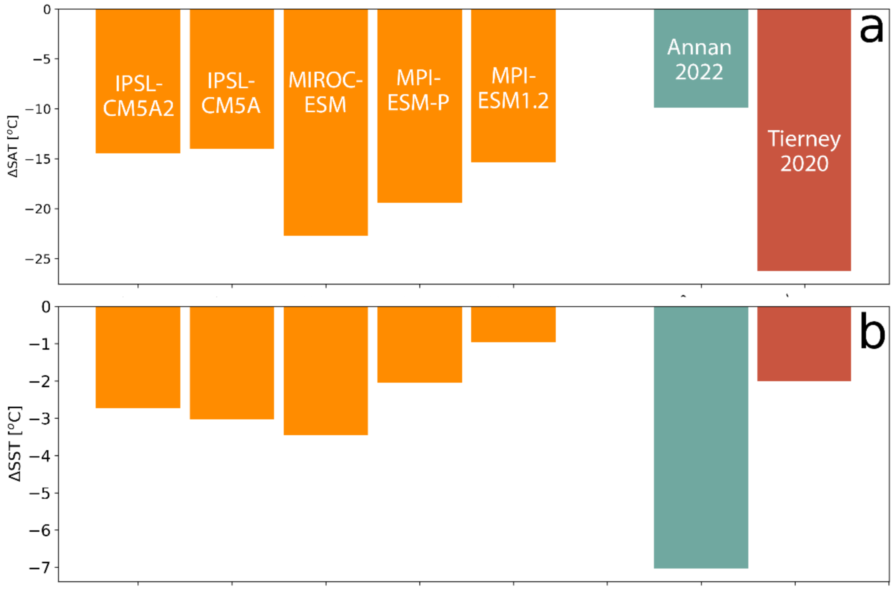

***Figure 1**: a: Near-surface atmospheric temperature anomalies at sea level during the LGM relative to the pre-industrial period averaged over the BKIS region, in the domain defined using the icemask from DATED1 at 21k for the 5 GCMs used to force GRISLI, as well as for the reconstructions of Annan et al. (2022) and Tierney et al. (2020). b: Same as (a), but for the Greenland Sea surface temperatures (see Fig. S1). For panel b, the labels of each box are the same as in panel a.*

2.2.3 Climate forcing index along the last deglaciation

2.2.3.1 Construction of the deglacial climate index

To reconstruct the climate evolution from the LGM to 10 ka, we relied on two transient climate simulations performed with the global circulation model CCSM3 (Liu et al., 2009) and the Earth system model of intermediate complexity iLOVECLIM (Bouttes et al., 2023). Hereafter, these simulations are referred to as the TRACE21k and iLOVECLIM respectively.

To perform the transient simulations, Bouttes et al. (2023) and Liu et al. (2009) forced their climate model (iLOVECLIM and CCSM3 respectively) in the same way, accounting for variations in greenhouse gases and astronomical parameters. However, one of the main differences lies in the reconstructed ice sheet that is used as a boundary condition of the deglaciation experiment. The TRACE21k simulation was based on ICE-5G (Peltier, 2004), whereas the iLOVECLIM simulation used the ICE-6G_C reconstruction (Peltier et al., 2015), which refines regional ice thickness and shifts the timing of deglaciation, notably by incorporating a more rapid ice loss during MWP1A to better align with sea-level observations (Peltier et al., 2014). Moreover, in iLOVECLIM, both the ice-sheet extent and volume are updated every 1000 years, whereas in TRACE21k, only the ice volume is updated at the same frequency as in iLOVECLIM (i.e., the ice-sheet extent remains fixed at LGM conditions throughout the simulation). The two simulations also differ in their treatment of freshwater fluxes from ice-sheet melting into the ocean. TRACE21k applies a scenario specifically designed to reproduce abrupt deglaciation events, whereas in iLOVECLIM, we chose to use simulations in which the release of freshwater fluxes is not considered, because when freshwater fluxes are included, the Atlantic Meridional Overturning Circulation is no longer active. Differences in both experimental protocols (TRACE21k and iLOVECLIM) lead to discrepancies in the simulated evolution of atmospheric and oceanic temperatures by the iLOVECLIM and CCSM3 models. Bouttes et al. (2023) also support this analysis, highlighting that the use of different ice-sheet reconstructions results in differences in both the amplitude and timing of the deglaciation. Moreover, the two simulations differ in their temporal resolution. Indeed, iLOVECLIM provides annual outputs while TRACE21k provides data every 10 years.

We did not use the direct outputs from iLOVECLIM or TRACE21k to force GRISLI because we were unable to construct a consistent ice sheet at the LGM with these two climate forcings. Instead, we chose to build an index based on the outputs of the deglaciation experiments run with both models. In this way, we obtain a spatially varying index computed at each grid point of the GRISLI domain, allowing us to represent the dynamics of the local climate. This approach differs from the classical method based on the use of an index derived from an ice core (Charbit et al., 2002; Huybrechts et al., 2002; Quiquet et al., 2018), which imposes the same dynamics across the entire domain.

The temporal climate indices $I_{T_{iL/TR}}(t,x,y)$ are defined as follows:

$$I_{T_{iL/TR}}(t,x,y) = \frac{T_{iL/TR}(t,x,y) - T_{iL/TR}(PI,x,y)}{T_{iL/TR}(LGM,x,y) - T_{iL/TR}(PI,x,y)} \quad (4)$$

where $T_{iL/TR}(t,x,y)$, $T_{iL/TR}(LGM,x,y)$ and $T_{iL/TR}(PI,x,y)$represent respectively the values at the point (x,y) of the atmospheric surface or oceanic 3D temperatures at the LGM and the PI periods and at time t, calculated with the iLOVECLIM (iL) or TRACE21k (TR) simulation. The atmospheric and oceanic indices range from 0 to 1, where 1 corresponds to LGM conditions and 0 to PI conditions. To prevent excessively large warming or cooling (for example, to prevent ocean temperatures from falling below the freezing point), the index was constrained between −2 and 2. Because GRISLI corrects atmospheric temperatures using a lapse rate, we adjusted the surface air temperatures simulated by iLOVECLIM and TRACE21k to sea level when calculating the atmospheric index. This avoids to count twice the vertical temperature correction during our simulations.

https://doi.org/10.5194/egusphere-2026-1137
Preprint. Discussion started: 7 April 2026

2.2.3.2 Transient climate forcing derived from the climate index

To build an evolving climate along the last deglaciation, we generate transient atmospheric and oceanic forcings using the $I_{T_{iL/TR}}(t,x,y)$ index between two climate snapshots, LGM and pre-industrial, from the selected PMIP models. The surface atmospheric temperatures and ocean temperatures at each oceanic level of the ocean column are then calculated at each time step as follows:

$$T_{iL/TR}\ (t,x,y) = T(PI,x,y) * \left(1 - I_{T_{iL/TR}}(t,x,y)\right) + T(LGM,x,y) * I_{T_{iL/TR}}(t,x,y) \qquad (5)$$

where $T_{iL/TR}\ (t,x,y)$ is the temperature at time t at the point (x,y), T(PI,x,y) and T(LGM,x,y) are the temperatures during the pre-industrial period and at the LGM simulated by the PMIP models. The salinity and precipitation are calculated in the same way. For the ocean temperature, we also set a lower bound corresponding to the freezing point.

The evolution of the atmospheric and oceanic temperatures calculated by the PMIP3/PMIP4 models with the use of the iLOVECLIM and the TRACE21k indices from the LGM to 10 ka is shown in Figures 2a and 2b. The main differences between the two indices is mainly due to discrepancies between the iLOVECLIM and TRACE21k simulations, as described in Bouttes et al. (2023) and Liu et al. (2009) respectively.

iLOVECLIM shows an earlier and more pronounced atmospheric warming compared to TRACE21k, with a relatively gradual warming. In contrast, with TRACE21k, the temperature does not rise before 17 ka and shows an abrupt increase at the time of the MWP1A, around 14 ka. The earlier and larger warming in iLOVECLIM suggests a stronger atmospheric response during the deglaciation. At the end of the deglaciation experiments, iLOVECLIM and TRACE21k show a significant temperature difference of ~10°C. However, this difference gradually decreases around 8 ka (not shown) as iLOVECLIM simulates a cooling of atmospheric temperatures (Bouttes et al., 2023) whereas TRACE21K remains stable (Liu et al., 2009). Similar differences are observed in subsurface ocean temperatures. While both indices produce long-term warming, their temporal evolution differs significantly. In the TRACE21k simulation, ocean temperatures start rising around 14 ka, coinciding with the MWP1A. On the other hand, the iLOVECLIM simulation shows a gradual but steady warming beginning much earlier until 14ka and shows a temporary cooling phase during the MWP1A. The difference between the two indices is likely due to whether or not freshwater fluxes from ice sheet melt are considered, as explained above. At the end of the BKIS deglaciation, both indices converge towards a similar evolution, with ocean temperatures rising continuously.

https://doi.org/10.5194/egusphere-2026-1137
Preprint. Discussion started: 7 April 2026

2.2.3 Climate forcing compared to reconstuctions

To assess the validity of the index method, we also compared our results with the reconstructions available at the time the experiments were conducted. In Figure 2c, we plotted the evolution of atmospheric temperature anomalies reconstructed thanks to data assimilation by Osman et al. (2021) above the BKIS, along with the evolution of surface temperatures anomalies computed in the same region using the index method (unlike in Figure 2a, here the atmospheric temperatures are not adjusted to sea level in order to be compared with the reconstruction of Osman et al., 2021). First, the atmospheric temperature anomaly reconstructed by Osman et al. (2021) appears relatively constant between 21 and 17 ka, following a similar evolution as that calculated using the TRACE21k index. A strong warming is then observed in the reconstructions from 17 ka onward, reaching the same anomaly values as those calculated with the iLOVECLIM index from ~16 ka. Finally, at 10 ka, a difference of ~5°C is found between the reconstructions and the atmospheric temperatures reconstructed with iLOVECLIM, whereas the TRACE21k-based temperatures underestimate the warming by more than 10°C compared to the reconstructions. Overall, atmospheric temperatures calculated with the iLOVECLIM index appear to overestimate the warming at the onset of deglaciation (21–15 ka), whereas those calculated with TRACE21k show an underestimation from 17 ka to 10 ka.

We also compared the evolution of subsurface ocean temperature anomalies with those reconstructed from the MD01-2461 (Peck, 2016) sediment core, located off the present-day British coast (Fig. 2d). Although the sediment core is not located exactly within the BKIS region, it provides valuable information on North Atlantic oceanic variability during the deglaciation. The reconstructions show a cooling between 21 and 17 ka, consistently with the subsurface temperatures calculated using the TRACE21k index. This cooling is followed by a strong warming at 17 ka. Between 15.5 and 13, the reconstructed temperature anomalies follow a similar trend to that derived from the iLOVECLIM index. By 10 ka, all three curves converge toward the same temperature anomaly. In contrast, the reconstructions exhibit greater temporal variability, particularly when compared with the temperatures derived from the iLOVECLIM index.

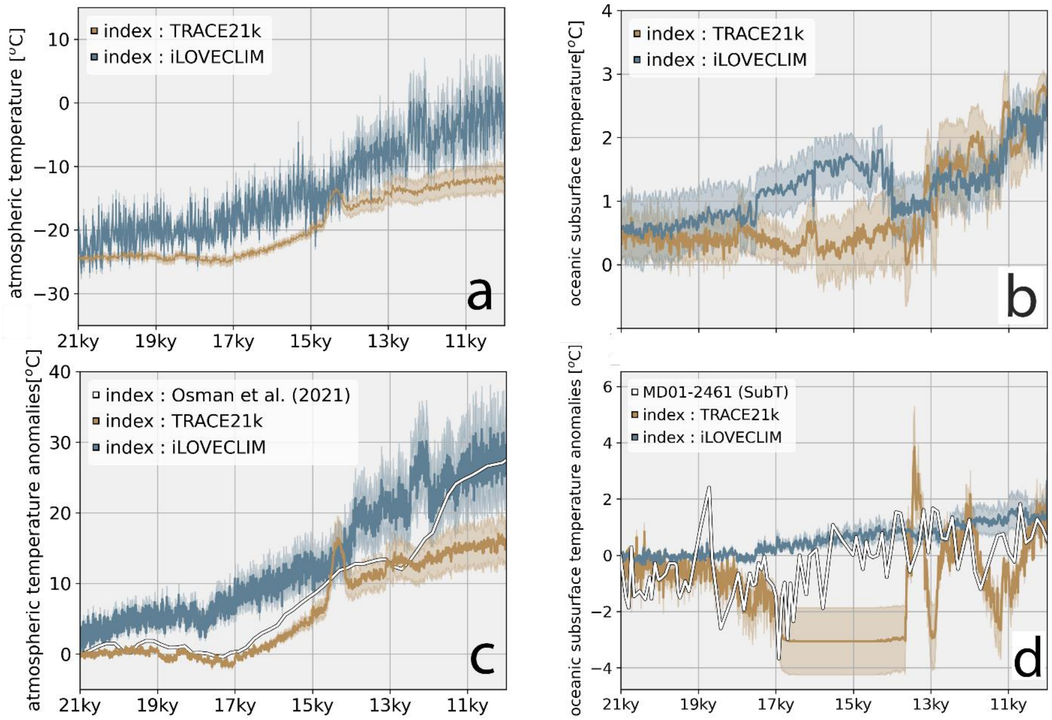

***Figure2:** a: Evolution of the PMIP3/PMIP4 multi-model mean atmospheric temperature at sea level over the BKIS region, in the domain defined using the icemask from DATED1 at 21ka, computed using the iLOVECLIM (blue) or TRACE21k (brown) climate indices. b: Evolution of the PMIP3/PMIP4 multi-model mean ocean temperature in the Barents Sea, averaged over depths between 200 and 750 m, computed using the iLOVECLIM (blue) or TRACE21k (brown) climate indices. c: Evolution of the PMIP3/PMIP4 multi-model mean atmospheric temperature anomalies over the BKIS region, computed using the iLOVECLIM (blue) or TRACE21k (brown) climate indices. The white curve shows atmospheric temperature anomalies over the BKIS region derived from data assimilation (Osman et al., 2021). d: Evolution of the PMIP3/PMIP4 multi-model mean ocean temperature anomalies in the Greenland Sea, averaged over depths between 100 and 200 m, computed using the iLOVECLIM (blue) or TRACE21k (brown) climate indices. The white curve shows subsurface ocean temperature anomalies at 150 m depth derived from a sediment core located off the present-day British coast (Peck, 2016). In the 4 panels, the shaded areas indicate the standard deviation across the five PMIP3/PMIP4 models.*

2.4 Experimental setup

We performed 5 spin-up experiments over 100,000 years, forced by a constant LGM climate coming from the 5 selected GCMs. The simulations start from an ice-free state with the eustatic sea-level set at 120 m below the present one and the initial bedrock topography is based on the present-day ETOPO1 dataset (Amante, 2009).

https://doi.org/10.5194/egusphere-2026-1137
Preprint. Discussion started: 7 April 2026

Then, we conducted 10 reference simulations of the BKIS deglaciation (21 to 10 ka), one for each climatic index applied to the climates simulated by the five GCMs (see Table S5), by varying sea level according to the reconstructions of Waelbroeck et al. (2002).

To assess the relative contributions of atmospheric and oceanic forcings and to investigate the role of mechanical instabilities, we conducted four additional sets of experiments, each designed to isolate specific processes forced by the iLOVECLIM index.

1. In the first series of experiments, we fixed the atmospheric temperatures at their LGM values while allowing ocean temperatures to vary, thus removing any atmospheric influence on the ice-sheet evolution (DEGLA-ATM-LGM). This provides a baseline to isolate the specific impact of oceanic forcing.
2. In the second series of experiments (DEGLA-NOBMELT), basal melting beneath the ice shelves was set to zero, eliminating ocean-induced melting. Here, atmospheric conditions were allowed to vary following the iLOVECLIM index.
3. We conducted a third series of experiments, DEGLA-NOBMELT-NOGL, in which we set the basal melting to zero and removed the analytical parameterization of grounding line flux (Tsai et al., 2015). This formulation can induce strong grounding line retreat, particularly over retrograde bed slopes such as those commonly found beneath BKIS (Amante et al., 2009, see Fig. S1), by amplifying the flux with increasing ice thickness. By eliminating this parameterization, we artificially reduce such flux-driven instabilities, and we isolate the role of oceanic forcing in our experiments.
4. However, even in the absence of sub-shelf melting or explicit ice flux at the grounding line, the ocean has an impact on the ice sheet simply because of flotation. Notably, switching from grounded to floating ice produces a strong change in the basal friction and therefore in the ice dynamics. For this reason, in the last series of experiments, we conducted a series of idealized experiments (DEGLA-NOSL), in which grounding line migration was entirely cancelled by imposing an artificially low sea level of -1000 m relative to present-day. As this sea level is far below the bedrock across the domain, no floating points remains. This allows to eliminate basal melt, the ice flux at the grounding line and calving.
5. To assess the potential for abrupt and irreversible retreat of the BKIS, we conducted a set of sensitivity experiments in which atmospheric temperatures and sea level were held constant at selected stages of the deglaciation (15.5, 15, 14.5, and 14 ka), while oceanic forcing remained fixed at its LGM state. For each experiment, once the target age was reached, the atmospheric climate index was fixed until the end of the simulation. This design allows us to isolate the impact of atmospheric warming on ice-sheet dynamics.
6. Finally, to test the sensitivity of the chosen basal melting parameterization, we run an additional sensitivity experiment following the DEGLA-ATM-LGM design, but with amplified basal melting at the grounding line.

https://doi.org/10.5194/egusphere-2026-1137
Preprint. Discussion started: 7 April 2026

For these six new series of experiments, the initial state is the same as in the reference simulations and we allow the ice sheet to calve when the relevant conditions are met (i.e. when ice thickness becomes less than 250m, see section 2.1). The objective of these experiments is to highlight the respective roles of atmospheric warming, basal melting beneath ice shelves, grounding line flux, and grounding line retreat due to flotation in the retreat of the BKIS during the last deglaciation.

3 Results

3.1 Ice sheet geometry at the LGM

The DATED-1 database (Hughes et al., 2016) provides a comprehensive collection of dated climate archives allowing the reconstruction of the BKIS extent every 1,000 years from 25 to 10 ka. The GLAC-1D (Tarasov et al., 2014, Abe-Ouchi et al., 2015) and ICE-6G_C reconstructions, based on an inverse modeling approach constrained by GPS data, relative sea level, and geomorphological evidence, provide ice extent and ice-sheet topography for at least 21 ka (Fig. S4). For the remainder of the study, we use the DATED-1 dataset to compare simulated ice extent. We also use the GLAC-1D and ICE-6G_C reconstructions to assess ice volume evolution. A detailed comparison of the spin-up simulations with these reconstructions is provided in the Supplement (Fig. S2).

3.2 Ice sheet geometry during the last deglaciation (21ka to 10ka)

For simulations forced with the iLOVECLIM index, the ice volume shows a continuous retreat between 21 and ~12 ka (depending on the PMIP model used to force GRISLI), with a marked acceleration of ice loss from ~14 ka onward (see Fig. 3a). This phase corresponds to a loss of about 40% of the total ice mass over 500 years, equivalent to a SLE of ~3 m over the same period. This rapid retreat is of the same order of magnitude as that inferred by Brendryen et al. (2020) from analyses of marine sediment cores. The diminution of ice volume along the deglaciation is broadly consistent with the ICE-6G_C reconstruction and with GLAC1D, except for a slight disagreement at the onset of deglaciation, where GLAC1D indicates a temporary increase in ice volume. Regarding ice-sheet extent, the simulations show a similar pattern, with a steady decrease followed by an accelerated decline from 14 ka. The evolution of ice extent generally matches the trends of the DATED-1 and GLAC1D reconstructions, which also show an accelerated retreat around 14 ka, with a reduction of about 50% of the ice extent over a few centuries. In contrast, the ICE-6G_C reconstruction displays a constant decrease in ice extent from 21 to 14 ka, followed by a period of stabilization between 14 and 11 ka, and then a rapid retreat between 11 and 10 ka.

Simulations using the TRACE21k index, by contrast, fail to reproduce the observed deglaciation patterns, mainly due to the delayed warming (see figure 2).

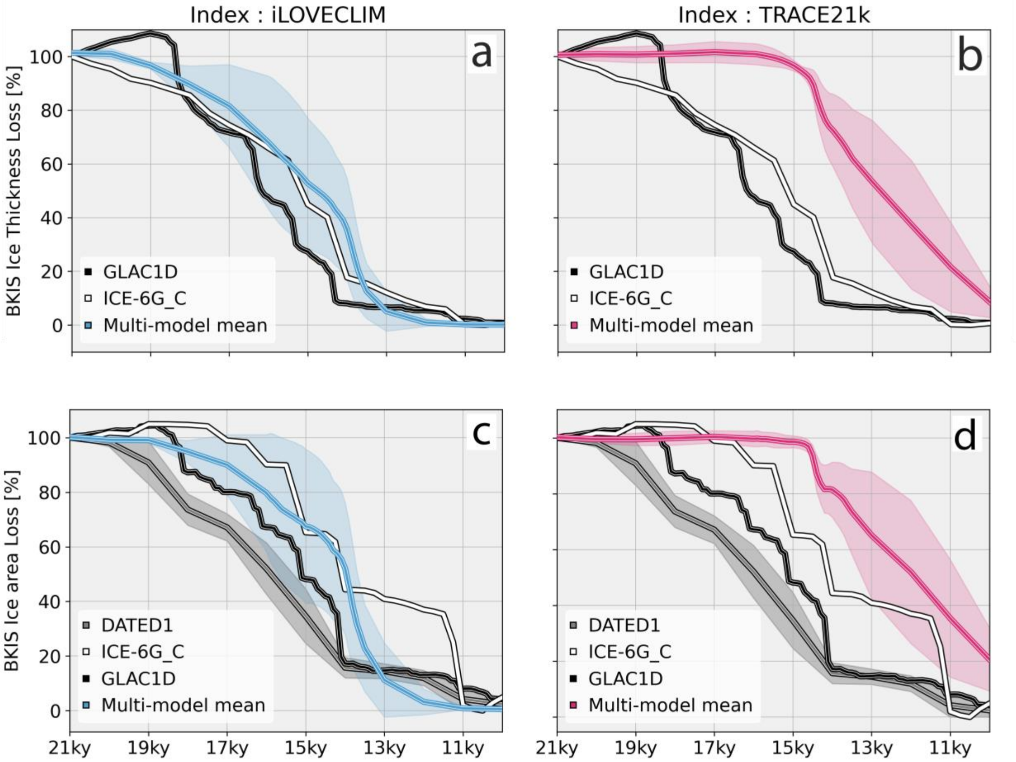

__Figure 3:__ a: Multi-model mean of the ice thickness loss in the BKIS region relative to the ice thickness of the LGM ice sheet, using the iLOVECLIM index (0% indicate 100% ice loss) compared to the GLAC1D (black) and ICE-6G_C (white) reconstructions. The label in the y axis is the loss of ice volume relative to its initial volume. b: Same as a, but with the TRACE21k index. The shaded area corresponds to the standard deviation of the ice volume between the 5 GCMs. c: same as a but for the ice extent compared to GLAC1D (black), ICE-6G_C (white) and DATED1 (grey) reconstructions. The blue shaded area corresponds to the standard deviation of the ice area between the 5 GCMs and the grey shaded area corresponds to the min and max DATED1 scenario. d: same as b but for the ice extent.

When examining in more detail the BKIS retreat at the scale of the ice sheet, we observe that, in the eastern part of BKIS, the evolution of the simulated ice extent is delayed compared to the DATED-1 reconstructions (Fig. 4), whatever the choice of the climatic index. The mismatch between our GRISLI simulations and the reconstructions could partly be explained, by the fact that the initial states we built (see Fig. S3) overestimate the ice extent in this region. which consequently leads to a delayed retreat of the ice sheet during deglaciation. This overestimated ice extent may be attributed to the climate forcings derived from PMIP simulations. In particular, the ice-sheet reconstructions used as boundary conditions in GCM simulations can imprint an enhanced regional cooling that favors ice expansion in the GRISLI simulations. This effect may also be amplified by the projection of the ice-sheet reconstructions onto the coarser GCM grid, which can artificially spread the ice-sheet mask and therefore produce a cooling signal that is too spatially extended.

https://doi.org/10.5194/egusphere-2026-1137
Preprint. Discussion started: 7 April 2026

Conversely, in the Bjørnøyrenna region, simulations performed with the iLOVECLIM index show a retreat starting between 18 and 16 ka, consistent with DATED-1. Except for the Svalbard and Primorsky regions (i.e., the areas above sea level; see Fig. S1b), for simulations forced by the iLVOECLIM index, melting ends around 12 ka in all simulations, except for the one forced by MIROC-ESM, whereas reconstructions indicate complete melting around 14 ka (see Fig. S5). This discrepancy is likely due to the large surface temperature anomaly simulated by MIROC-ESM (see Fig. 1).

Our simulations consistently show that BKIS deglaciation generally begins in regions in contact with the ocean, such as the Bjørnøyrenna and Svyataya Anna ice streams (Figs. 4, S1 and S5), where some confined ice shelves emerge due to the geographic configuration. This pattern suggests that oceanic processes may play a major role in controlling the dynamics of the BKIS in line with previous studies (Petrini et al., 2020; Alvarez-Solas et al., 2019). Because of this, we explore in the following sections the processes behind this retreat by examining the respective effects of the ocean, atmosphere, and other physical mechanisms.

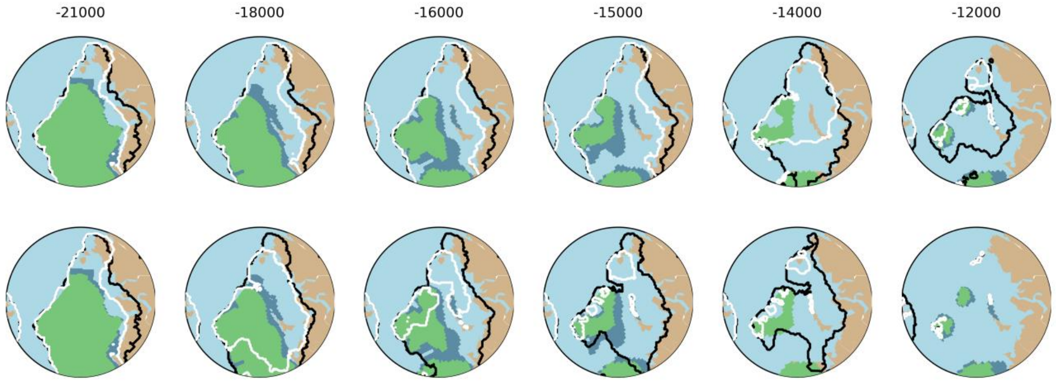

Figure 4*: Top: The blue shape represents the ice extent provided by the max scenario of DATED-1 at different time periods and the green shape to the min scenario. The black lines show the maximum ice extent from the 5 references simulations performed with TRACE21k and the white line the minimum ice extent at each time step. down: same as up but for iLOVECLIM index*

3.3 Atmospheric forcing, oceanic forcing?

All the experiments presented in this section are based on the iLOVECLIM index, as it offers a better agreement with the reconstructions when used in the GRISLI reference simulations. In the following, we only present the results obtained with the MPI-ESM1.2 GCM forcing, as it simulates the most consistent LGM ice volume and extent with the reconstructions when used to force GRISLI (Figs S2-S3). Results obtained with the other GCMs are available in the Supplement (Figs S8-S11).

Figures 5a and 5b show the ice thickness of grounded ice and ice shelves at different key dates for the reference and the DEGLA-ATM-LGM (i.e. atmospheric temperatures fixed to their LGM values) simulations. In the absence of atmospheric warming after the LGM, no significant ice-

https://doi.org/10.5194/egusphere-2026-1137
Preprint. Discussion started: 7 April 2026

sheet retreat is simulated. Our results suggest that the increase in ocean temperatures alone is not sufficient to trigger the retreat of BKIS, highlighting the crucial role of atmospheric warming in initiating the BKIS deglaciation (van Aalderen et al., 2024).

The main difference between the results of the reference and DEGLA-NOBMELT (no basal melting under the ice shelves) experiments lies in the extent of the ice shelves (Figs. 5a, 5c). As expected, as atmospheric temperatures rise, some confined ice shelves appear, and due to the absence of basal melting, the simulated ice shelves extend farther throughout the deglaciation compare to the reference simulation. This larger extent enhances the buttressing effect which reduces the ice flux at the grounding line with respect to the reference experiment hence increases upstream grounded ice thickness. While the buttressing effect seems to have only a moderate influence on the position of the grounding line at the beginning of the deglaciation, the effect begin to be clearly visible between 14 ka and 13.5 ka. Compared to the reference simulation, the total ice loss at 13.5 ka is reduced by about 10% relative to the reference ice volume at the same date.

Moreover, when the ice flux at the grounding line is ignored (Tsai et al., 2015, DEGLA-NOBMELT-NOGL), the grounding line retreat is further delayed compared to DEGLA-NOBMELT (Figs. 5a, 5d). This emphasizes the sensitivity of grounding line dynamics to this prescribed flux. Compared to the reference simulation, in this experiment, the ice loss is reduced by about 17% at 13.5 ka relative to the initial ice volume. Finally, by fully eliminating the ocean's influence (DEGLA-NOSL), we observe an even more pronounced delay in the retreat of the BKIS compared to both DEGLA-NOBMELT and DEGLA-NOBMELT-NOGL (Fig. 5e), underscoring the critical role of the transition from grounded to floating ice in controlling marine-based ice sheet deglaciation dynamics (see Figs. 5a and 5e). In this case, at 13.5 ka, the ice loss is reduced by about 45% relative compared to the reference.

Consequently, this set of experiments highlights the primary role of variations in atmospheric conditions in triggering the abrupt retreat of the marine sector of BKIS. However, unlike van Aalderen et al. (2024), we also emphasize the indirect role of the ocean, notably the significant impact of the transition from grounded to floating ice, as well as the crucial influence of the ice flux at the grounding line, which plays a key role in controlling the dynamics of the marine sector retreat of BKIS.

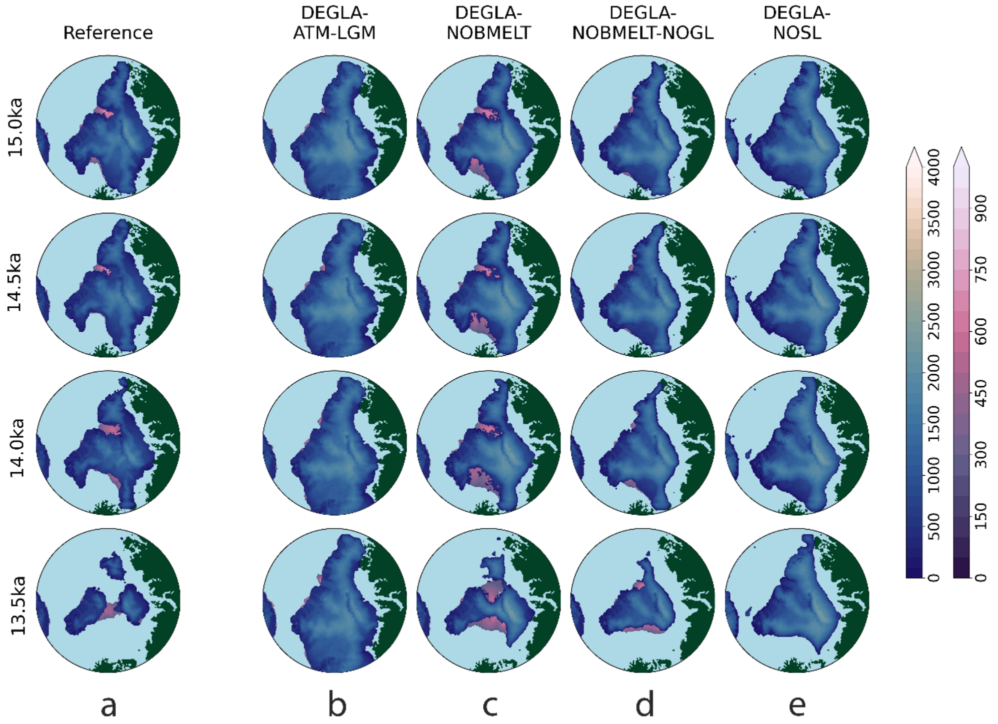

***Figure 5**: Ice thickness (in meters) of grounded ice (blue shaded areas) and ice shelves (pink shaded areas) at different time steps using the iLOVECLIM index, the MPI-ESM1.2 forcing and β_{min} = 10 Pa.s.m^{-1} for the reference (a), b: the DEGLA-ATM-LGM; c: DEGLA-NOBMELT; d: DEGLA-NOBMELT-NOGL and e: DEGLA-NOSL.*

3.4 MISI-driven retreat of the BKIS

We have previously shown that, in our simulations, the BKIS retreat exhibits a strong acceleration starting around 14.5 ka (Fig. 3) and demonstrated that grounding line migration plays an important role in driving the BKIS retreat. This raises the question as to whether this behaviour could be associated with a rapid and an irreversible retreat driven by a mechanical instability, more specifically by a MISI.

We performed sensitivity experiments to test whether the BKIS can undergo an abrupt and irreversible retreat. Atmospheric temperature and sea level were fixed at key deglaciation stages (15.5, 15, 14.5 and 14 ka), while ocean forcing was kept at its LGM state. This setup, applied across five GCMs using the iLOVECLIM index, isolates the role of atmospheric warming and assesses its ability to trigger a MISI.

Figure 6a shows the evolution of the atmospheric index through time for the different simulations. It clearly illustrates that the atmospheric forcing warms during the deglaciation (i.e.,

https://doi.org/10.5194/egusphere-2026-1137
Preprint. Discussion started: 7 April 2026

the closer the index is to 0, the closer the climate is to an interglacial state). Once the key date is reached, the climate becomes constant over time.

The simulated ice volume evolution (Fig. 6b) reveals different responses depending on the date on which the climate stabilises. When atmospheric warming is halted at 15.5 ka, the increase in surface melt is insufficient to trigger an abrupt retreat of the BKIS. Although ice loss continues, mainly due to the temperature-elevation feedback, the response remains moderate and no large-scale destabilization occurs.

In contrast, when the atmospheric index is stabilized at 15 ka, 14.5 ka, or 14 ka, a rapid and substantial ice volume loss is simulated, despite the absence of further atmospheric warming. This indicates that BKIS has already crossed a critical threshold prior to stabilization and ice retreat therefore continues under constant climatic conditions. Compared with the reference simulation, where the ice sheet has completely retreated around 12 ka, approximately 1/3 of the total ice volume remains in the stabilization experiments. This residual ice is primarily located in regions situated above sea level, such as Svalbard and Primorsky regions which are less sensitive to marine ice instability.

The contrast between the 15.5 ka experiment and the other stabilization experiments suggests the existence of a critical SMB threshold. When atmospheric warming is halted at 15.5 ka, this threshold has not yet been exceeded, and BKIS does not exhibit instability behaviour. However, in the experiments stabilized at 15 ka or later, the BKIS is already unstable, and ice loss continues for the rest of the deglaciation. These results show that once a critical SMB threshold is exceeded, the BKIS retreat becomes abrupt and irreversible.

However, this abrupt retreat could be due to a marine instability or to the elevation-temperature feedbacks. To tackle this question, we performed an extra experiment. This experiment follows exactly the same protocol as the simulation stabilized at 14.5 ka, except that the lapse rate is set to 0 °C km^{-1} (instead of 7 °C km^{-1}) once the stabilization date is reached. This allows to hold constant the atmospheric temperature. We show that, even without this elevation-temperature feedback, the ice sheet still undergoes a substantial retreat, but smaller than in the simulation with a lapse rate set to 7 °C km^{-1} (see Fig. 6b). This suggests that the process in the BKIS retreat is driven by the MISI, with the elevation-temperature feedback amplifying the marine instability. In this scenario, the initial increase in atmospheric temperatures triggers a marine instability. This instability leads to ice thinning, which in turn amplifies local atmospheric temperatures through the elevation–temperature feedback, accelerating the marine instability and sustaining further abrupt retreat.

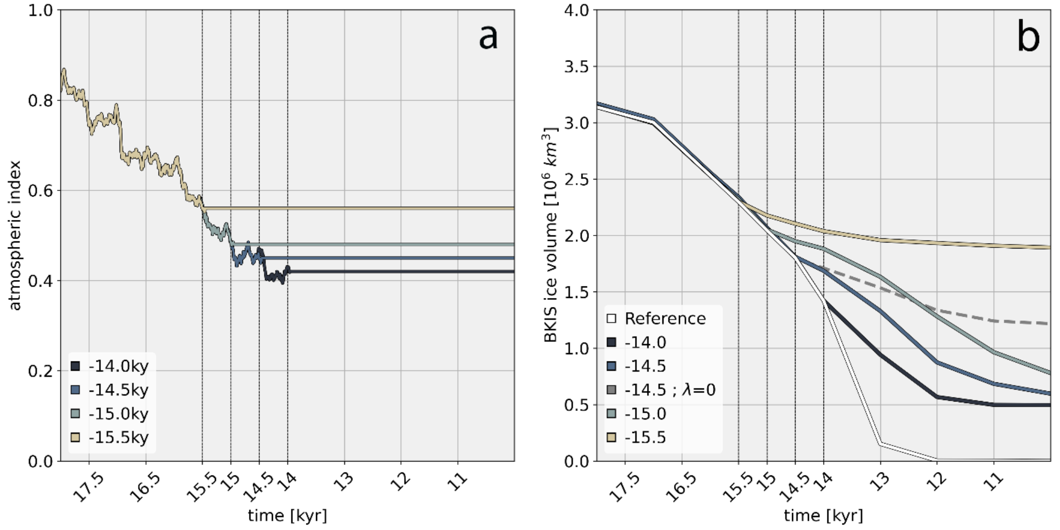

Figure 6: *a: Evolution of the atmospheric index over time for the different stabilized experiments. b: Evolution of the BKIS ice volume for the different stabilized experiments averaged over the 5 GMCs, using the iLOVECLIM index. Solid lines represent simulations with a lapse rate of 7 °C km^{-1} throughout, while dashed lines show simulations where the lapse rate is 7 °C km^{-1} between –21 and 14.5 ka, then set to 0 °C km^{-1} until the end of the simulation.*

Then, to quantify the roles of the marine instability and SMB changes in the BKIS retreat, we conducted an analysis of the deglaciation of the Bjørnøyrenna region using the reference experiment forced by MPI-ESM1.2 and the iLOVELCIM index (DEGLA-MPI1.2-iLOVECLIM-10). To do so, we plotted the respective contributions of SMBB (the sum between surface mass balance and basal melting; see Eq. 1) and dynamic processes (represented by the ice flux divergence ∇(UH) in Eq. 1) to the variation in ice thickness at the onset of a significant ice stream retreat (i.e., between 14.5 and 14 ka, Fig. 7).

The simulation shows a significant decrease in ice thickness in the BKIS region, with mean values of the ice thickness variation greater than 600m between 14.5 and 14ka (Fig. 7a). SMBB contributes only marginally to the total ice loss, with values less than 100m (Fig. 7a). In contrast, dynamic processes are responsible for a loss of more than 600m in 500 years (Fig. 7a), particularly in the interior of the ice sheet, where the SMBB is positive. This illustrates a noticeable acceleration of the ice flow triggered by the dynamical processes which propagates upstream. In the interior of the BKIS region, ΔH has the same pattern as -∇(UH), meaning that the dynamical loss is the primary cause of the decrease in ice thickness. These results show that the increase in atmospheric temperatures put BKIS in a state where dynamical processes can occurs, primarily leading to the melting of the marine part of BKIS. The mechanism can be explained as follows:

atmospheric warming reduces ice thickness near the grounding line, making the ice to float and triggering the retreat of the grounding line. Since the underlying bedrock has a retrograde slope (see Fig. S1b), the retreat of the ice towards the interior of the ice sheet enhances the ice flux at the grounding line, causing a further retreat and resulting in a self-sustained and accelerated ice sheet collapse. The sequence of these processes suggested by our results is consistent with a MISI mechanism initiated by the atmospheric warming and leading to the retreat of BKIS.

To assess whether BKIS retreat is amplified by a MISI, we performed the same analysis for the DEGLA-NOSL simulation, in which the ocean's influence is fully removed. By completely suppressing ocean forcing, we also eliminate the mechanical instability associated with the MISI. Figure 7b presents the analysis of the different components (SMBB and dynamical processes) at several key time steps and shows a clear delay in deglaciation compared to the reference simulation (Fig. 7a). In this case, when the oceanic influence is entirely removed, the BKIS retreat is largely delayed compared to the reference simulation, thereby highlighting the major role of the MISI in driving BKIS retreat in the reference experiments.

In the end, the stabilized experiments, combined with the updated analysis of the various processes, demonstrated that the BKIS retreat is both abrupt and irreversible (on the deglaciation timescale). Our results indicate that this behaviour is primarily controlled by a MISI, whereby grounding line retreat triggers a positive feedback, with the elevation–temperature feedback further amplifying the retreat. This mechanism leads to accelerated ice loss once a critical threshold is crossed (between 15ka and 14.5ka in our simulations). These findings provide evidence that the rapid retreat of the BKIS is mechanically driven, rather than solely forced by climate variations.

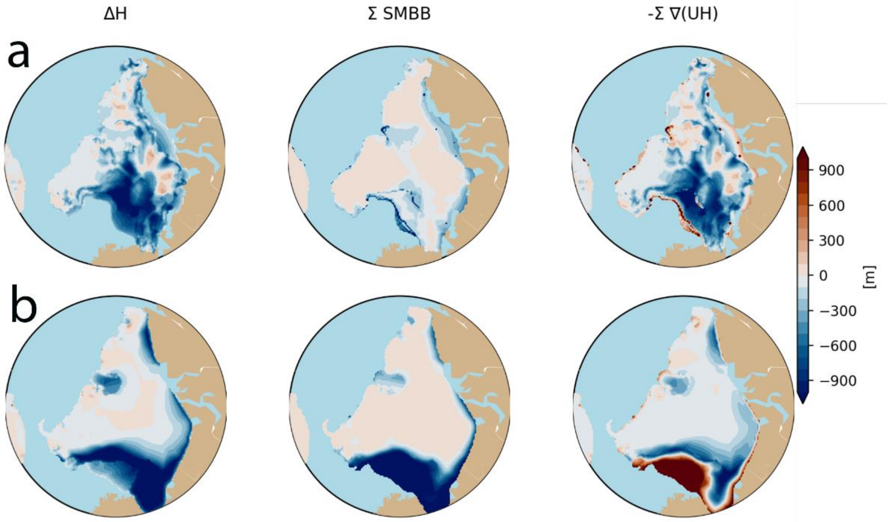

***Figure** 7: a: Respective roles of SMBB versus ice dynamics for the DEGLA-MPI1.2-iLOVECLIM experiment between 14.5ka and 14 ka. left/ Variation in ice thickness (in m yr-1) middle/ variation in* $SMBB$ *(=* $SMB\text{-}bmelt$*) and right/ integral of the opposite of the divergence (i.e. convergence)*

https://doi.org/10.5194/egusphere-2026-1137
Preprint. Discussion started: 7 April 2026

of the ice flux: negative values correspond to a divergence of the ice flux and thus to ice loss caused by dynamical processes. b: same as a but for the DEGLA-NOSL experiment between 14ka and 13.5ka.

4 Discussions

For comparison with the previous study by van Aalderen et al. (2024), we reconstructed evolving climate scenarios reproducing the observed dynamics of the ice volume loss and ice extent during the last deglaciation, and we also performed simulations designed to identify the respective contributions of climate and dynamical processes. In addition, we carried out new experiments specifically designed to demonstrate the abrupt and irreversible retreat of BKIS. These simulations go beyond the previous study, providing a more realistic and detailed assessment of the processes driving the BKIS deglaciation. As a result, they allow us to identify mechanisms of the ice sheet that were not captured in van Aalderen et al. (2024), offering significant new insights into the BKIS behavior during the last deglaciation.

These new experiments allow us to highlight the dominant role of atmospheric forcing in driving the BKIS retreat at the onset of the deglaciation, while showing that oceanic temperatures play a much more limited role to trigger the retreat of the ice sheet. The weak sensitivity of BKIS to oceanic temperatures at the onset of deglaciation is likely due to the limited extent of confined ice shelves in our simulations. It is worth considering whether the initial LGM configuration of the BKIS underestimates the extent of confined ice shelves, particularly in the Bjørnøyrenna region. However, ice sheet reconstructions (DATED-1, ICE-6G_C, and GLAC-1D) indicate that confined ice shelves were indeed very limited at the LGM (see Fig. S4). This can be explained by the region’s geographical configuration, and notably by the abrupt transition between the continental shelf and the deep ocean basin between Norway and Svalbard (see Fig. S1b). As a result, the ice sheet was fully grounded on the continental shelf at the LGM, both in our simulations and in the reconstructions. Consequently, at the start of deglaciation, BKIS had very few confined ice shelves, minimizing its sensitivity to oceanic forcing. According to our simulations, the atmospheric warming triggered an initial retreat of the grounding line in the Bjørnøyrenna region, leading to the formation of confined ice shelves and increased the ice sheet’s sensitivity to oceanic conditions. However, the relatively coarse resolution of GRISLI (20 km × 20 km) may limit the representation of small confined ice shelves, potentially leading to an underestimation of the ocean’s impact. Higher-resolution simulations would allow a more accurate assessment of the formation of such confined ice shelves and help determine whether, if present, they significantly influence BKIS dynamics.

Our relatively weak sensitivity of the BKIS to oceanic warming contrasts with previous modeling studies (Petrini et al., 2020; Alvarez-Solas et al., 2019). Differences in basal melting parameterization between ice-sheet initialization and deglaciation experiments in those studies may partly explain the stronger ocean-driven retreat reported in these studies as explained in van Aalderen et al. (2024). In the present work, besides applying a consistent basal melting parameterization between the equilibrium initialization and the deglaciation simulations, we performed experiments in which atmospheric and oceanic perturbations were imposed separately (see Fig. 5). This experimental design allows a clearer identification of the processes

https://doi.org/10.5194/egusphere-2026-1137
Preprint. Discussion started: 7 April 2026

controlling BKIS retreat, in contrast to Petrini et al. (2020) where both forcings were varied simultaneously. However, it is well established that increasing ocean temperatures can have a significant impact on marine-based ice sheets (Pritchard et al., 2012), and the choice of basal melt parameterization may affect the ice sheet sensitivity to oceanic variations (Burgard et al., 2022). Moreover, the selected PMIP model may simulate a too slow ocean warming to significantly enhance the BKIS retreat. To test whether our results might be influenced by the basal melt parameterization or by the PMIP ocean temperature forcing, we conducted additional simulations in which ocean temperatures were artificially increased by 10 °C (see Fig. S12), producing basal melt rates at the grounding line in the Bjørnøyrenna region on the order of 30 m yr^{-1}, and consequently approaching the upper theoretical basal melt limit highlighted in Favier et al. (2019). Despite this substantial increase, no significant retreat occurred during the deglaciation, further supporting the conclusion that atmospheric warming is the primary driver of grounding line instability in our simulations (Fig. S12).

Moreover, basal friction between the ice sheet and the bedrock is a poorly constrained parameter. As a result, it may be underestimated in our configuration, which could influence the simulated sensitivity of the BKIS to climatic variations. Consequently, to assess the ice sheet's sensitivity to basal friction, we performed additional simulations using different values for the lower bound of the friction coefficient. In addition to β_{min} = 10 $Pa.s.m^{-1}$ we conducted the same reference experiment with β_{min} = 50 or 100 $Pa.s.m^{-1}$ (see Figs. S2, S3, S6 and S7). Increasing the lower bound of the basal friction coefficient reduces ice sliding over the bedrock. Overall, the results indicate that basal friction has only a limited impact on the BKIS dynamics, as these additional simulations exhibit the same behavior than the references simulations.

Constructing the initial states through an equilibrium experiment forced by a LGM climate can also influence the simulated retreat dynamics of the BKIS. Unlike a simulated ice sheet evolving, transiently over long timescales, an ice sheet equilibrated under an LGM climate tends to develop a geometry fully adjusted to cold climatic conditions. This can lead, among other things, to a more pronounced glacio-isostatic depression of the bedrock and warm bias. Both effects are likely to modify grounding line stability and, consequently, the sensitivity of the ice sheet to MISI during deglaciation. However, as shown in van Aalderen et al. (2024), the use of initial states constructed with a transient method does not lead to any major differences in the response of the BKIS to variations in both atmospheric and oceanic conditions.

Another source of uncertainty concerns the absence of hydrofracturing in GRISLI. This process has been shown to play potentially an important role in the destabilization of ice shelves and the deglaciation of marine ice sheets (DeConto and Pollard 2016, Goffin et al., 2025). Its implementation in our modeling framework would likely amplify ice retreat in response to atmospheric warming, thereby reinforcing our conclusion that atmospheric temperatures were the primary driver of BKIS retreat.

The representation of glacio-isostatic adjustment (GIA) in our simulations could also bring some uncertainties. In GRISLI, bedrock deformation is computed using an Elastic Lithosphere–Relaxed Asthenosphere (ELRA) model with a relaxation time of 3 kyr. However, regional studies suggest that longer relaxation times may be more appropriate in some areas. For example, analyses of the Ångermanland relative sea-level record indicate decay times with a 2σ lower bound above 4 kyr (Nordmann et al., 2015). A longer relaxation time would delay the bedrock uplift following ice retreat and therefore reduce the attenuation of retrograde bed slopes during deglaciation. In such a case, the grounding line would remain longer on retrograde slopes, which could enhance retreat through MISI. Therefore, using a longer relaxation time would likely favor a stronger retreat of the BKIS and would not contradict the mechanisms highlighted in our simulations.

Finally, Brendryen et al. (2020) conclude, based on marine sediment core, that several mechanisms played a key role in the BKIS retreat, including surface melting, temperature–elevation feedback and MISI. They suggest that the BKIS retreat was likely triggered by a rapid increase in subsurface temperatures occurring shortly before MWP-1A, while atmospheric temperatures appear to have remained constant. Our simulations forced by the iLOVECLIM index align with the deglaciation timing proposed by Brendryen et al. (2020), showing a decrease in ice volume equivalent to about 3 m of sea level in just 500 years. Moreover, our results broadly support the mechanisms suggested by these authors, except for the triggering mechanisms of the rapid BKIS retreat around 15 ka, which, in our simulations, is mainly caused by an increase in atmospheric temperatures. These new, partially contradictory results raise several questions: is the oceanic forcing used to drive GRISLI truly representative of the conditions at the start of deglaciation? Is the subsurface warming before the MWP-1A, as mentioned by Brendryen et al. (2020), sufficient on its own to trigger the retreat of the BKIS? We encourage future studies to address these questions in order to better constrain the relative roles of atmospheric and oceanic forcing in driving the BKIS retreat.

5. Concluding remarks

Using different climatic forcings as inputs to the GRISLI ice-sheet model combined with an evolving climatology, and by varying basal sliding-law parameters, we investigated the mechanisms responsible for the retreat of the BKIS. Removing basal melting beneath ice shelves enhanced the buttressing effect and reduced grounding line ice flux, lowering total ice loss by ~10%. Suppressing the analytical ice flux at the grounding line further delayed retreat, reducing ice loss by 17%, while fully disabling flotation led to a 45% reduction. Each of this steps progressively slowed the grounding line retreat, highlighting the critical role of oceanic processes in BKIS deglaciation. Our simulations also show that BKIS retreat was abrupt and largely irreversible, with a marked acceleration between 15 and 14.5 ka, indicating a rapid transition once destabilization conditions were met. Moreover, we show that these marine ice sheet instabilities were initiated by rising atmospheric temperatures and later amplified by the elevation–temperature feedback, rather than by direct ocean warming, suggesting a strong coupling between atmospheric forcing and ice sheet dynamics.

While oceanic temperatures are not the main trigger of the BKIS retreat in our simulations, we corroborate previous studies on the essential role of the ocean in sustaining retreat through the MISI mechanism. This study further highlights that other factors, especially atmospheric warming, can initiate MISI, emphasizing the need for a more integrated approach in future marine ice sheet modeling. In particular, while basal melting beneath ice shelves remains the dominant driver of the retreat of the West Antarctic Ice Sheet retreat, the influence of rising atmospheric temperatures in the future should be carefully considered, as they may play a decisive role in triggering instabilities. Overall, our results underline the importance of jointly considering oceanic and atmospheric forcings to fully understand past and future marine ice sheet behavior.

Acknowledgments

Victor van Aalderen is funded by the French National Research Agency (Grant: ANR-22-CE01-0024). We acknowledge the World Climate Research Programme's Working Group on Coupled Modelling, which is responsible for the Paleoclimate Modelling Intercomparison Project (PMIP) for producing and making available their model output. We also thank Nathaelle Bouttes and Zhengyu Liu for providing access to their transient simulation. This work benefited from productive exchanges with N. Jourdain, D. Swingedouw, Jorge Alvarez-Solas and Florence Colleoni. This study has received funding from the Agence Nationale de la Recherche - France 2030 as part of the PEPR TRACCS programme under grant number ANR-22-EXTR-0010

Author contributions

All authors designed the study. VvA performed the numerical experiments. All authors contributed to the analysis of model results. VvA and SC wrote the paper, with input from AQ and CD.

Data availability

The source data of the experiments presented in the main text of the paper are available from the Zenodo repository at https://doi.org/10.5281/zenodo.15394253 (van Aalderen et al., 2025)

References

Abe-Ouchi, A., Saito, F., Kageyama, M., Braconnot, P., Harrison, S. P., Lambeck, K., Otto-Bliesner, B. L., Peltier, W. R., Tarasov, L., Peterschmitt, J.-Y., and Takahashi, K.: Ice-sheet configuration in the CMIP5/PMIP3 Last Glacial Maximum experiments, Geosci. Model Dev., 8, 3621–3637, https://doi.org/10.5194/gmd-8-3621-2015, 2015.

Adloff, M., Reick, C. H., and Claussen, M.: Earth system model simulations show different feedback strengths of the terrestrial carbon cycle under glacial and interglacial conditions, Earth Syst. Dynam., 9, 413–425, https://doi.org/10.5194/esd-9-413-2018, 2018.

Alvarez-Solas, J., Banderas, R., Robinson, A., and Montoya, M.: Ocean-driven millennial-scale variability of the Eurasian ice sheet during the last glacial period simulated with a hybrid ice-sheet–shelf model, Clim. Past, 15, 957–979, https://doi.org/10.5194/cp-15-957-2019, 2019.

Amante, C.: ETOPO1 1 Arc-Minute Global Relief Model: Procedures, Data Sources and Analysis, https://doi.org/10.7289/V5C8276M, 2009.

Annan, J. D., Hargreaves, J. C., and Mauritsen, T.: A new global surface temperature reconstruction for the Last Glacial Maximum, Clim. Past, 18, 1883–1896, https://doi.org/10.5194/cp-18-1883-2022, 2022.

Applegate, P. J., Kirchner, N., Stone, E. J., Keller, K., and Greve, R.: An assessment of key model parametric uncertainties in projections of Greenland Ice Sheet behavior, The Cryosphere, 6, 589–606, https://doi.org/10.5194/tc-6-589-2012, 2012.

Bouttes, N., Lhardy, F., Quiquet, A., Paillard, D., Goosse, H., and Roche, D. M.: Deglacial climate changes as forced by different ice sheet reconstructions, Clim. Past, 19, 1027–1042, https://doi.org/10.5194/cp-19-1027-2023, 2023.

Brendryen, J., Haflidason, H., Yokoyama, Y., Haaga, K. A., and Hannisdal, B.: Eurasian Ice Sheet collapse was a major source of Meltwater Pulse 1A 14,600 years ago, Nat. Geosci., 13, 363–368, https://doi.org/10.1038/S51561-020-0567-4, 2020.

Brondex, J., Gagliardini, O., Gillet-Chaulet, F., and Durand, G.: Sensitivity of grounding line dynamics to the choice of the friction law, J. Glaciol., 63, 854–866, https://doi.org/10.1017/jog.2017.51, 2017.

Burgard, C., Jourdain, N. C., Reese, R., Jenkins, A., and Mathiot, P.: An assessment of basal melt parameterisations for Antarctic ice shelves, The Cryosphere, 16, 4931–4975, https://doi.org/10.5194/tc-16-4931-2022, 2022.

DeConto, R. M. and Pollard, D.: Contribution of Antarctica to past and future sea-level rise, Nature, 531, 591–597, https://doi.org/10.1038/nature17145, 2016.

Deschamps, P., Durand, N., Bard, E., Hamelin, B., Camoin, G., Thomas, A. L., Henderson, G. M., Okuno, J., and Yokoyama, Y.: Ice-sheet collapse and sea-level rise at the Bølling warming 14,600 years ago, Nature, 483, 559–564, https://doi.org/10.1038/nature10902, 2012.

Dufresne, J.-L., Foujols, M.-A., Denvil, S., Caubel, A., Marti, O., Aumont, O., Balkanski, Y., Bekki, S., Bellenger, H., Benshila, R., Bony, S., Bopp, L., Braconnot, P., Brockmann, P., Cadule, P., Cheruy, F., Codron, F., Cozic, A., Cugnet, D., de Noblet, N., Duvel, J.-P., Ethé, C., Fairhead, L., Fichefet, T., Flavoni, S., Friedlingstein, P., Grandpeix, J.-Y., Guez, L., Guilyardi, E., Hauglustaine, D., Hourdin, F., Idelkadi, A., Ghattas, J., Joussaume, S., Kageyama, M., Krinner, G., Labetoulle, S., Lahellec, A., Lefebvre, M.-P., Lefevre, F., Levy, C., Li, Z. X., Lloyd, J., Lott, F., Madec, G., Mancip, M., Marchand, M., Masson, S., Meurdesoif, Y., Mignot, J., Musat, I., Parouty, S., Polcher, J., Rio, C., Schulz, M., Swingedouw, D., Szopa, S., Talandier, C., Terray, P., Viovy, N., and Vuichard, N.: Climate change projections using the IPSL-CM5 Earth System Model: from CMIP3 to CMIP5, Clim Dyn, 40, 2123–2165, https://doi.org/10.1007/s00382-012-1636-1, 2013.

Fairbanks, R. G.: A 17,000-year glacio-eustatic sea level record: influence of glacial melting rates on the Younger Dryas event and deep-ocean circulation, Nature, 342, 637–642, https://doi.org/10.1038/342637a0, 1989.

Goelzer, H., Nowicki, S., Payne, A., Larour, E., Seroussi, H., Lipscomb, W. H., Gregory, J., Abe-Ouchi, A., Shepherd, A., Simon, E., Agosta, C., Alexander, P., Aschwanden, A., Barthel, A., Calov, R., Chambers, C., Choi, Y., Cuzzone, J., Dumas, C., Edwards, T., Felikson, D., Fettweis, X., Golledge, N. R., Greve, R., Humbert, A., Huybrechts, P., Le clec'h, S., Lee, V., Leguy, G., Little, C., Lowry, D. P., Morlighem, M., Nias, I., Quiquet, A., Rückamp, M., Schlegel, N.-J., Slater, D. A., Smith, R. S., Straneo, F., Tarasov, L., van de Wal, R., and van den Broeke, M.: The future sea-level contribution of the Greenland ice sheet: a multi-model ensemble study of ISMIP6, The Cryosphere, 14, 3071–3096, https://doi.org/10.5194/tc-14-3071-2020, 2020.

Goffin, A. A., Tarasov, L., Benediktsson, Í. Ö., and Licciardi, J. M.: Growth and decay of the Iceland Ice Sheet through the last glacial cycle, https://doi.org/10.5194/egusphere-2025-5319, 10 November 2025.

Goldberg, D., Holland, D. M., and Schoof, C.: Grounding line movement and ice shelf buttressing in marine ice sheets, J. Geophys. Res., 114, 2008JF001227, https://doi.org/10.1029/2008JF001227, 2009.

Hughes, A. L. C., Gyllencreutz, R., Lohne, Ø. S., Mangerud, J., and Svendsen, J. I.: The last Eurasian ice sheets – a chronological database and time-slice reconstruction, DATED-1, Boreas, 45, 1–45, https://doi.org/10.1111/bor.12142, 2016.

Huybrechts, P.: Sea-level changes at the LGM from ice-dynamic reconstructions of the Greenland and Antarctic ice sheets during the glacial cycles, Quaternary Science Reviews, 21, 203–231, https://doi.org/10.1016/S0277-3791(01)00082-8, 2002.

Intergovernmental Panel on Climate Change: Climate Change 2021 – The Physical Science Basis: Working Group I Contribution to the Sixth Assessment Report of the Intergovernmental Panel on Climate Change, 1st ed., Cambridge University Press, https://doi.org/10.1017/9781009157896, 2023.

Le Meur, E. and Huybrechts, P.: A comparison of different ways of dealing with isostasy: examples from modelling the Antarctic ice sheet during the last glacial cycle, Ann. Glaciol., 23, 309–317, https://doi.org/10.3189/S0260305500013586, 1996.

Liu, Z., Otto-Bliesner, B. L., He, F., Brady, E. C., Tomas, R., Clark, P. U., Carlson, A. E., Lynch-Stieglitz, J., Curry, W., Brook, E., Erickson, D., Jacob, R., Kutzbach, J., and Cheng, J.: Transient Simulation of Last Deglaciation with a New Mechanism for Bølling-Allerød Warming, Science, 325, 310–314, https://doi.org/10.1126/science.1171041, 2009.

Mauritsen, T., Bader, J., Becker, T., Behrens, J., Bittner, M., Brokopf, R., Brovkin, V., Claussen, M., Crueger, T., Esch, M., Fast, I., Fiedler, S., Fläschner, D., Gayler, V., Giorgetta, M., Goll, D. S., Haak, H., Hagemann, S., Hedemann, C., Hohenegger, C., Ilyina, T., Jahns, T., Jimenéz-de-la-Cuesta, D., Jungclaus, J., Kleinen, T., Kloster, S., Kracher, D., Kinne, S., Kleberg, D., Lasslop, G., Kornblueh, L., Marotzke, J., Matei, D., Meraner, K., Mikolajewicz, U., Modali, K., Möbis, B., Müller, W. A., Nabel, J. E. M. S., Nam, C. C. W., Notz, D., Nyawira, S., Paulsen, H., Peters, K., Pincus, R., Pohlmann, H., Pongratz, J., Popp, M., Raddatz, T. J., Rast, S., Redler, R., Reick, C. H., Rohrschneider, T., Schemann, V., Schmidt, H., Schnur, R., Schulzweida, U., Six, K. D., Stein, L., Stemmler, I., Stevens, B., Storch, J., Tian, F., Voigt, A., Vrese, P., Wieners, K., Wilkenskjeld, S., Winkler, A., and Roeckner, E.: Developments in the MPI-M Earth System Model version 1.2 (MPI-ESM1.2) and Its Response to Increasing CO_2, J. Adv. Model. Earth Syst., 11, 998–1038, https://doi.org/10.1029/2018MS001400, 2019.

Mercer, J. H.: Antarctic Ice and Interglacial High Sea Levels, Science, 168, 1605–1606, https://doi.org/10.1126/science.168.3939.1605.b, 1970.

Nordman, M., Milne, G., and Tarasov, L.: Reappraisal of the Ångerman River decay time estimate and its application to determine uncertainty in Earth viscosity structure, Geophysical Journal International, 201, 811–822, https://doi.org/10.1093/gji/ggv051, 2015.

Laske, G.: A global digital map of sediment thickness, Eos Trans. AGU, 78, F483, 1997

Osman, M. B., Tierney, J. E., Zhu, J., Tardif, R., Hakim, G. J., King, J., and Poulsen, C. J.: Globally resolved surface temperatures since the Last Glacial Maximum, Nature, 599, 239–244, https://doi.org/10.1038/S51586-021-03984-4, 2021.
Peck, V. L.: Sea surface and subsurface temperature reconstruction for sediment core MD01-2461, https://doi.org/10.1594/PANGAEA.861240, 2016.

Peltier, W. R.: GLOBAL GLACIAL ISOSTASY AND THE SURFACE OF THE ICE-AGE EARTH: The ICE-5G (VM2) Model and GRACE, Annu. Rev. Earth Planet. Sci., 32, 111–149, https://doi.org/10.1146/annurev.earth.32.082503.144359, 2004.

Peltier, W. R., Argus, D. F., and Drummond, R.: Space geodesy constrains ice age terminal deglaciation: The global ICE-6G_C (VM5a) model: Global Glacial Isostatic Adjustment, J. Geophys. Res. Solid Earth, 120, 450–487, https://doi.org/10.1002/2014JB011176, 2015.

Petrini, M., Colleoni, F., Kirchner, N., Hughes, A. L. C., Camerlenghi, A., Rebesco, M., Lucchi, R. G., Forte, E., Colucci, R. R., Noormets, R., and Mangerud, J.: Simulated last deglaciation of the

Barents Sea Ice Sheet primarily driven by oceanic conditions, Quaternary Science Reviews, 238, 106314, https://doi.org/10.1016/j.quascirev.2020.106314, 2020.

Pollard, D. and DeConto, R. M.: Description of a hybrid ice sheet-shelf model, and application to Antarctica, Geosci. Model Dev., 5, 1273–1295, https://doi.org/10.5194/gmd-5-1273-2012, 2012.

Quiquet, A., Dumas, C., Ritz, C., Peyaud, V., and Roche, D. M.: The GRISLI ice sheet model (version 2.0): calibration and validation for multi-millennial changes of the Antarctic ice sheet, Geosci. Model Dev., 11, 5003–5025, https://doi.org/10.5194/gmd-11-5003-2018, 2018.

Ritz, C., Rommelaere, V., and Dumas, C.: Modeling the evolution of Antarctic ice sheet over the last 420,000 years: Implications for altitude changes in the Vostok region, J. Geophys. Res., 106, 31943–31964, https://doi.org/10.1029/2001JD900232, 2001.

Sepulchre, P., Caubel, A., Ladant, J.-B., Bopp, L., Boucher, O., Braconnot, P., Brockmann, P., Cozic, A., Donnadieu, Y., Dufresne, J.-L., Estella-Perez, V., Ethé, C., Fluteau, F., Foujols, M.-A., Gastineau, G., Ghattas, J., Hauglustaine, D., Hourdin, F., Kageyama, M., Khodri, M., Marti, O., Meurdesoif, Y., Mignot, J., Sarr, A.-C., Servonnat, J., Swingedouw, D., Szopa, S., and Tardif, D.: IPSL-CM5A2 – an Earth system model designed for multi-millennial climate simulations, Geosci. Model Dev., 13, 3011–3053, https://doi.org/10.5194/gmd-13-3011-2020, 2020.

Seroussi, H., Nowicki, S., Payne, A. J., Goelzer, H., Lipscomb, W. H., Abe-Ouchi, A., Agosta, C., Albrecht, T., Asay-Davis, X., Barthel, A., Calov, R., Cullather, R., Dumas, C., Galton-Fenzi, B. K., Gladstone, R., Golledge, N. R., Gregory, J. M., Greve, R., Hattermann, T., Hoffman, M. J., Humbert, A., Huybrechts, P., Jourdain, N. C., Kleiner, T., Larour, E., Leguy, G. R., Lowry, D. P., Little, C. M., Morlighem, M., Pattyn, F., Pelle, T., Price, S. F., Quiquet, A., Reese, R., Schlegel, N.-J., Shepherd, A., Simon, E., Smith, R. S., Straneo, F., Sun, S., Trusel, L. D., Van Breedam, J., van de Wal, R. S. W., Winkelmann, R., Zhao, C., Zhang, T., and Zwinger, T.: ISMIP6 Antarctica: a multi-model ensemble of the Antarctic ice sheet evolution over the 21st century, The Cryosphere, 14, 3033–3070, https://doi.org/10.5194/tc-14-3033-2020, 2020.

Sueyoshi, T., Ohgaito, R., Yamamoto, A., Chikamoto, M. O., Hajima, T., Okajima, H., Yoshimori, M., Abe, M., O'ishi, R., Saito, F., Watanabe, S., Kawamiya, M., and Abe-Ouchi, A.: Set-up of the PMIP3 paleoclimate experiments conducted using an Earth system model, MIROC-ESM, Geosci. Model Dev., 6, 819–836, https://doi.org/10.5194/gmd-6-819-2013, 2013.

Tarasov, L. and Richard Peltier, W.: Greenland glacial history and local geodynamic consequences, Geophysical Journal International, 150, 198–229, https://doi.org/10.1046/j.1365-246X.2002.01702.x, 2002.

Tarasov, L., Hughes, A., Gyllencreutz, R., Lohne, O. S., Mangerud, J., and Svendsen, J.-I.: The global GLAC-1c deglaciation chronology, meltwater pulse 1-a, and a question of missing ice, IGS

Symposium on Contribution of Glaciers and Ice Sheets to Sea-Level Change, IGS Symposium abstracts, 2014.

Tierney, J. E., Zhu, J., King, J., Malevich, S. B., Hakim, G. J., and Poulsen, C. J.: Glacial cooling and climate sensitivity revisited, Nature, 584, 569–573, https://doi.org/10.1038/S51586-020-2617-x, 2020.

Tsai, V. C., Stewart, A. L., and Thompson, A. F.: Marine ice-sheet profiles and stability under Coulomb basal conditions, J. Glaciol., 61, 205–215, https://doi.org/10.3189/2015JoG14J221, 2015.

van Aalderen, V., Charbit, S., Dumas, C., and Quiquet, A.: Relative importance of the mechanisms triggering the Eurasian ice sheet deglaciation in the GRISLI2.0 ice sheet model, Clim. Past, 20, 187–209, https://doi.org/10.5194/cp-20-187-2024, 2024.

van Aalderen, V.: Triggering dynamic instability in marine ice sheet via surface processes, https://doi.org/10.5281/ZENODO.15394253, 2025.

Waelbroeck, C., Labeyrie, L., Michel, E., Duplessy, J. C., McManus, J. F., Lambeck, K., Balbon, E., and Labracherie, M.: Sea-level and deep water temperature changes derived from benthic foraminifera isotopic records, Quaternary Science Reviews, 21, 295–305, https://doi.org/10.1016/S0277-3791(01)00101-9, 2002.